ADVANCED MATERIALS

bridge using two nanoparticle films (3 cm^2 geometric surface area, ~500 nm thick) immersed in aqueous 1.0 M $LiClO_4$ solution in a two terminal arrangement. Impedance spectra were measured from 0.1 Hz to 10 kHz and capacitance values were calculated as described previously [18].

Actuator Formation: Typically 250 μL of a 0.1 M solution of cystamine hydrochloride in water was added to 25 mL of a gold nanoparticle solution (2.5×10^{-4} M Au). The average diameter of the gold nanoparticles was approximately 16 nm (as measured by TEM). The cystamine hydrochloride induces rapid aggregation of the gold nanoparticles and the aggregates are filtered under vacuum onto a nanoporous polycarbonate track-etch membrane (PCTE) (Isopore, Millipore Corp., 10 μm thick, 200 nm nominal pore size). Film thickness was varied by changing the amount of nanoparticle solution used. For example, 25 mL of gold nanoparticle solution forms a 400 nm thick film of area 5 cm^2.

Actuation Experiments: Actuator strips of the nanoparticle film–PCTE composite material measuring 20 mm by 2 mm were placed in a 1.0 N KCl solution with a Pt/Pt-black counter and a standard calomel electrode (SCE) reference electrode. Electrical contact was made to the actuator strip via a press contact with a small clamp whose face had been lined with Pt foil, connected via a wire as the working electrode of the potentiostat. Area of the press contact was approximately 5 mm by 2 mm. Both triangular wave (100 $mV\,s^{-1}$) and square wave pulse potentials were applied using a Princeton Applied Research EG&G 263 potentiostat. The applied potential was in the range ±0.6 V. The bending response of the actuator under test was captured as digital video and analyzed manually in terms of deflection δ (Fig. 1a) as a function of time.

Received: December 2, 2002
Final version: February 10, 2003

[1] I. Z. Steinberg, A. Oplatka, A. Katchalsky, *Nature* **1966**, *210*, 568.
[2] R. H. Baughman, C. Cui, A. A. Zakhidov, Z. Iqbal, J. N. Barisci, G. M. Spinks, G. G. Wallace, A. Mazzoldi, D. De Rossi, A. G. Rinzler, O. Jaschinsky, S. Roth, M. Kertesz, *Science* **1999**, *284*, 1340.
[3] Y. Osada, H. Okuzaki, H. Hori, *Nature* **1992**, *355*, 242.
[4] S. Juodkazis, N. Mukai, R. Wakaki, A. Yamaguchi, S. Matsuo, H. Misawa, *Nature* **2000**, *408*, 178.
[5] R. H. Baughman, *Synth. Met.* **1996**, *78*, 339.
[6] R. Pelrine, R. Kornbluh, Q. Pei, *Science* **2000**, *287*, 836.
[7] *Electroactive Polymer (EAP) Actuators as Artificial Muscles, Reality, Potential, Challenges* (Ed: Y. Bar-Cohen), SPIE Press, Washington, DC **2001**.
[8] E. W. H. Jager, O. Inganäs, I. Lundström, *Science* **2000**, *288*, 2335.
[9] E. Smela, O. Inganäs, I. Lundström, *Science* **1995**, *268*, 1735.
[10] D. Dragoman, M. Dragoman, *Prog. Quantum Electron.* **2001**, *25*, 229.
[11] M. Lahav, C. Durkan, R. Gabai, E. Katz, I. Willner, M. E. Welland, *Angew. Chem. Int. Ed.* **2001**, *40*, 4095.
[12] *Metal Nanoparticles: Synthesis, Characterization and Applications.* (Eds: D. L. Feldheim, C. A. Foss Jr.), Marcel Dekker New York **2002**.
[13] A. N. Shipway, E. Katz, I. Willner, *ChemPhysChem* **2000**, *1*, 18.
[14] A. M. Moulin, S. J. O'Shea, M. E. Welland, *Ultramicroscopy* **2000**, *82*, 23.
[15] R. Raiteri, M. Grattarola, H.-J. Butt, P. Skládal, *Sens. Actuators, B* **2001**, *79*, 115.
[16] B. Raguse, J. Herrmann, G. Stevens, J. Myers, G. Baxter, K.-H. Müller, T. Reda, A. Molodyk, V. B. M. Braach-Maksvytis, *J. Nanopart. Res.* **2002**, *4*, 137.
[17] M. D. Musick, C. D. Keating, M. H. Keefe, M. J. Natan, *Chem. Mater.* **1997**, *9*, 1499.
[18] B. Raguse, V. Braach-Maksvytis, B. A. Cornell, L. G. King, P. D. J. Osman, R. J. Pace, L. Wieczorek, *Langmuir* **1998**, *14*, 648.
[19] G. G. Stoney, *Proc. R. Soc. London* **1909**, *A82*, 172.
[20] S. Tamulevicius, *Vacuum* **1998**, *51*, 127.
[21] Q. Pei, O. Inganäs, *J. Phys Chem.* **1992**, *96*, 10 507.
[22] J. Turkevich, P. C. Stevenson, J. Hillier, *Discuss. Faraday Soc.* **1951**, *11*, 55.
[23] G. Frens, *Nature (London), Phys. Sci.* **1973**, *241*, 20.

Fabrication of the MgC_xCo_3 Ternary Phase Encapsulated in Carbon Nanoflasks**

By *Rohit K. Rana*, *Xiao N. Xu*, *Yosef Yeshurun*, and *Aharon Gedanken**

The demonstration that magnetic nanoparticles can be encapsulated into protective carbon shells has initiated intensive research effort owing to the potential applications that these occluded materials could have in various fields.[1] These applications include a variety of uses such as magnetic data storage, magnetic toners in xerography, magnetic inks, ferrofluids, and contrast agents for magnetic resonance imaging.[1] The wrapping graphitic shell not only protects the core material from oxidation but also acts as a solid lubricant that can enable the high speed scan of a magnetic tape.

There have been various approaches to inserting magnetic and other materials into the graphitic shell. Among the various techniques conventional and modified arc-discharge processes are the usual methods for the synthesis of carbon-encapsulated metals or carbides. The most detailed studies in this area have been carried out by Saito et al.,[2] Seraphin et al.,[3] and Ruoff et al.[4] A substantial work concentrating mainly on the encapsulation of magnetic materials has also been carried out by Majetich and co-workers.[5] It has been found that different metals can have a profoundly different effect on the final shape, structure, and composition of the material produced in the arc-evaporation method. However, in all the cases filled nanoparticles are more commonly observed than filled nanotubes. Apart from the carbon-arc method, there have been other alternative methods such as pyrolysis,[6] the template technique,[7] and wet chemical methods[8] to insert metal or other interesting materials into carbon nanotubes or nanocages. So far the materials that could be encapsulated inside carbon nanotubes or nanocages have been restricted to pure metal or binary systems such as alloys and carbides. Here we report for the first time the formation of a ternary phase of MgC_xCo_3 occluded inside carbon nanoflasks. It is worth mentioning that the nickel analogue of MgC_xCo_3 is both superconducting and ferromagnetic with a critical temperature of 8 K (T_c).[9]

Nanoflasks belong to the carbon nanotube family and can be described as having an ovoid or bulbous base to which a narrower tubular part is attached.[10–12] Such nanostructures are prepared by thermally decomposing metal carbonyls in

[*] Prof. A. Gedanken, Dr. R. K. Rana
Department of Chemistry, Bar-Ilan University
Ramat-Gan 52900 (Israel)
E-mail: gedanken@mail.biu.ac.il
Dr. X. N. Xu, Prof. Y. Yeshurun
Department of Physics, Bar-Ilan University
Ramat-Gan 52900 (Israel)

[**] We thank the Israeli Ministry of Science, Culture and Sports for supporting this research via an Infrastructure grant. R.K.R thanks the Bar-Ilan Research Authority for his postdoctoral fellowship. A.G. thanks the German Ministry of Science through the Deutsche-Israel program, DIP, for its support.

  DOI: 10.1002/adma.200304690

the presence of magnesium granules that has a surface covering of magnesium hydroxide.[11] The carbon nanoflasks are generally obtained with encapsulated metallic cobalt present at their bulbous base. Here we describe a simple modification of the nanoflask synthesis procedure that lead to the formation of a ternary phase instead of cobalt encapsulated inside the nanoflask.

In Figure 1, the transmission electron microscopy images illustrate the characteristic flask-shaped feature of the carbon nanoflask, and visible at its base is the core filled with MgC_xCo_3. In the as-synthesized sample only a few carbon nanoflasks could be seen, as they were mostly covered by the catalytic particles (Fig. 1a). These impurities however, could be removed by HCl treatment after which the nanoflasks were clearly seen, as illustrated in the Figures 1b–d. In each nanoflask a sharp distinction between the occluded particle and the outer covering could be seen, suggesting that the particle is completely enclosed within the carbon shell. This was also confirmed by the fact that the MgC_xCo_3 particles could still be seen even after acid treatment of the sample (Figs. 1b,c). The sizes of the globular part of the nanoflask ranged from 100–900 nm and consisted of multiwalled graphitic shell, while the tubular parts extended up to a few micrometers. The outer diameter of the tubular part was found to be non-uniform throughout the length with a gradual decrease in the diameter from neck to tail. The percentage of nanoflasks of all the observed structures is approximately 20 %. However, as the nanoflasks are the only structures that carry the magnetic materials, it is possible that the nanoflask content can be enhanced by a magnetic separation technique, as has previously been demonstrated.[12]

Along with the filled nanoflasks, a few empty ones were also detected only in the acid-treated sample (Fig. 1d). The empty core might be a result of HCl reaction with the alloy particles. However, the filled nanoflasks indicate that complete coverage by the graphitic cage may effectively shield the inner materials from reacting with the acid. A similar phenomenon was also observed for the encapsulated cobalt analogue.[10,11] In some cases filling of the tubular part was also observed as shown in Figure 1c.

In order to obtain compositional and structural information on individual nanoflasks, selected area energy dispersive analysis of X-rays (SAEDAX) and electron diffraction (ED) analyses were performed on various selected parts, such as the globular base, neck, and tubular tail of the nanoflask. The SAEDAX scan from the globular part is shown in Figure 2a. It revealed that the acid-treated sample has a content of Mg and cobalt in an atomic ratio of 1:3.1, corresponding to the perovskite composition. However, finding the exact amount of carbon in the perovskite was difficult because the carbon content (Table 1) corresponds to the total amount of carbon

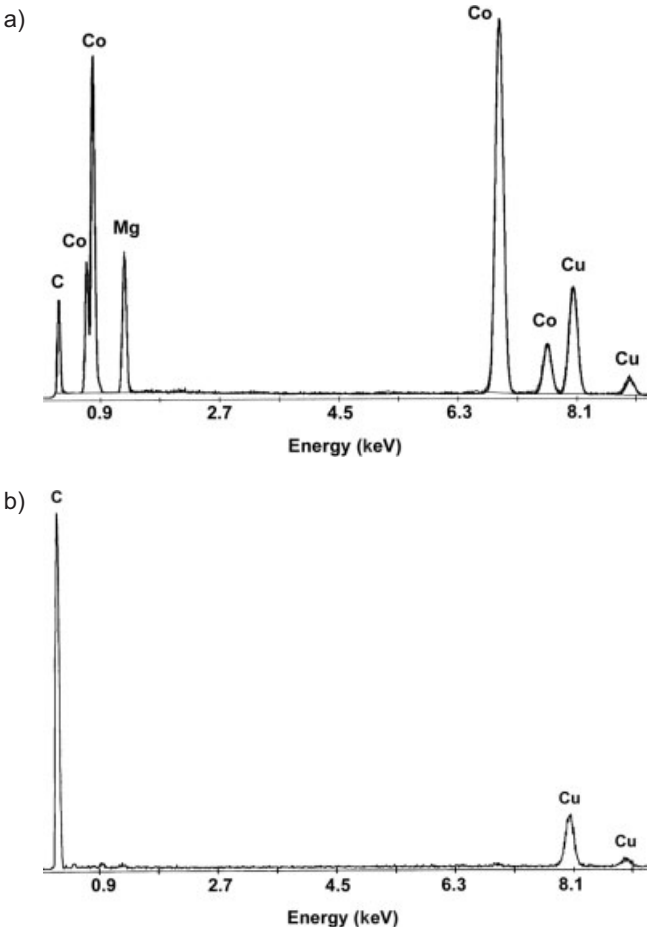

Fig. 2. The selected area EDAX of a) the globular base and b) the tail of the carbon nanoflask shown in Figure 3.

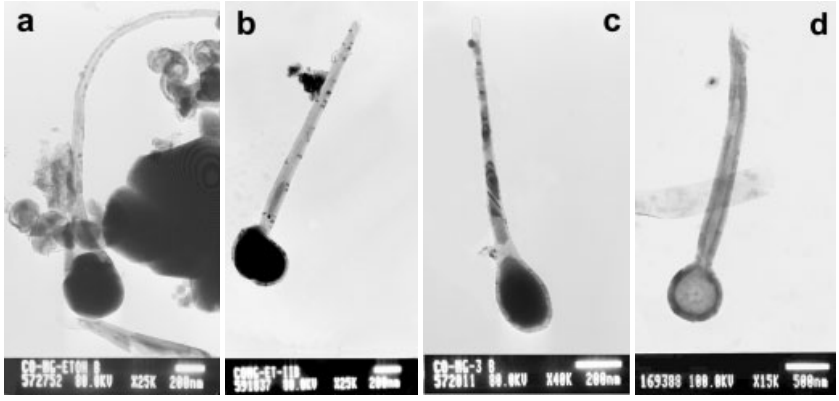

Fig. 1. Representative TEM images of the sample a) before acid-treatment and b–d) after acid-treatment.

ADVANCED MATERIALS

Table 1. Elemental composition of the globular part of the nanoflask as calculated from SAEDAX analyses.

Element	Atomic percentage [%]
C	41.1
Mg	14.1
Co	44.7

present both in the encapsulated material and the surrounding graphene layers. On the other hand, the SAEDAX scan from the neck and tail parts of the nanoflask showed that the composition of both the parts are similar with carbon as the only detected element (Fig. 2b). The SAED pattern of the globular part is shown in Figure 3b, depicting the presence of both spots and rings. The brightest innermost ring corresponded to

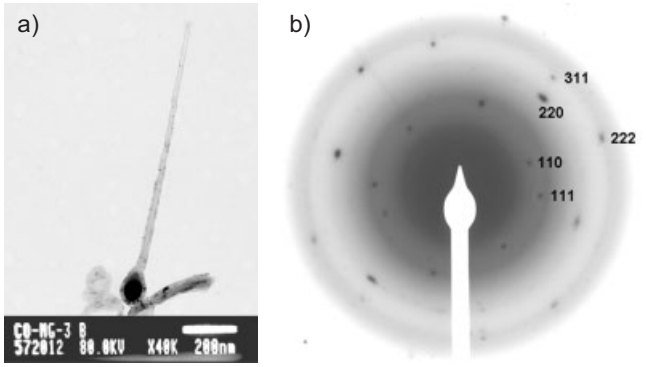

Fig. 3. a) TEM image of a carbon nanoflask and b) the corresponding SAED pattern obtained from the globular base of the carbon nanoflask.

the 002 reflection of hexagonal graphite. The sharp spots could be indexed by considering the $MgC_{0.5}Co_3$ structure. The appearance of clear spots indicates that the encapsulated material is highly crystalline. A comparison of the interlayer distance measured by ED with the known values is presented in Table 2.

Table 2. Summary of SAED data recorded from the globular part of the nanoflask.

Measured "*d*" (± 0.05 Å)	Known "*d*" [Å] [a]	Assignment (*hkl*)
2.66	2.70	110
2.17	2.20	111
1.40	1.35	220
1.20	1.15	311
1.14	1.10	222

[a] The interplanar distance "*d*" values are from the $MgC_{0.5}Co_3$ JCPDS file 29-0487.

The X-ray diffraction (XRD) patterns of the sample before and after acid-treatment are shown in Figure 4. The results clearly show the formation of an MgC_xCo_3 phase. The XRD peaks due to MgC_xCo_3 were indexed based on the available data for one of the compositions ($MgC_{0.5}Co_3$; JCPDS file: 29-0487), which has a face-centered cubic (fcc) crystal lattice. It is interesting to note that although the fcc phase does not

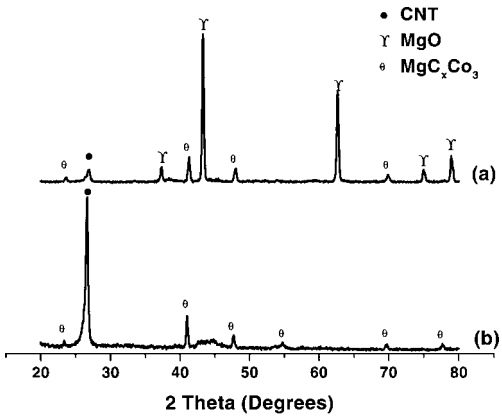

Fig. 4. X-ray diffractograms of a) the as-synthesized sample and b) the sample after acid treatment.

exist in the Mg–Co phase diagram, the presence of carbon stabilizes the MgC_xCo_3 phase in the fcc structure.[13] Apart from MgC_xCo_3 the XRD patterns also contain peaks due to graphite and magnesium oxide. The absence of metallic cobalt both in the as-synthesized and acid-treated samples indicates that the cobalt has been completely used in forming the ternary phase of MgC_xCo_3. As shown in Figure 4b, after acid-treatment the (002) graphitic peak became more prominent with the disappearance of dominant MgO peaks. From the graphitic (002) peak the average interlayer spacing was calculated to be 3.4 Å, corresponding to a turbostratic type of structural arrangement. In accordance with the transmission electron microscopy (TEM) observations, the MgC_xCo_3 peaks were found even after acid treatment, indicating that the particles are well covered by graphene layers. From CHN analysis the as-synthesized sample was found to have a carbon content of 11.3 wt.-%. After treatment with HCl the amount of material recovered from the products was 10.7 wt.-% and it had a carbon content of 78.5 wt.-%.

In order to understand the mechanism involved in the formation of a ternary phase the results have to be compared with those of the cobalt encapsulated analogue. There is a close morphological similarity between MgC_xCo_3 and Co encapsulated in carbon nanoflasks, thus indicating a similar kind of growth mechanism might be operative in both the cases. However, the important point to be noted here is the formation of MgC_xCo_3 instead of only cobalt, despite the fact that, apart from the temperature at which the reactions were carried out, the preparation methods are very similar. Cobalt encapsulation in carbon nanoflasks was achieved at 900 °C, while the formation of MgC_xCo_3 took place at 1000 °C. This clearly indicates that a strong interaction between Mg and cobalt leads to the formation of an alloy along with carbon only above 900 °C. From various analyses it had previously been demonstrated that the presence of Mg is very important for the fabrication of the unique shape of the nanoflasks.[11] According to the proposed mechanism[11] Mg first partially covers the cobalt particles generated from the thermal decomposition of $Co(CO)_3NO$. Then the CO disproportionation reaction over the exposed part of the metal initiates the

formation of carbon nanoflask. This was confirmed by the presence of magnesium only in the globular part but not in the tubular part. It was also observed that the magnesium not only helps shape the carbon nanoflasks, it also promotes the CO disproportionation reaction.[11]

Therefore it is possible that the initially adsorbed Mg further reacts with cobalt and the generated carbon at 1000 °C forming the ternary phase of MgC_xCo_3. Crucial to nanoflask formation is the amount of Mg that is used in the reaction mixture. When a mixture of Mg and MgO having 20 wt.-% Mg is used instead of "$Mg(OH)_2$ coated Mg granules" it results in the formation of carbon nanotubes rather than nanoflasks.[14] In the present case the amount of Mg is 85 wt.-%, part of which initially reacts with $Mg(OH)_2$ to generate the MgO support having electron-rich defect centers that can promote the CO disproportionation reaction over the cobalt catalyst.[11,14] The remaining Mg is then involved in covering the cobalt particles in such a way that it helps nucleate nanoflask formation.[11] The appearance of a flask-like feature is due to the bigger size of the cobalt particle compared to the diameter of the nanotube that grows from it.

Further studies were carried out to investigate the magnetic behavior of the occluded particles in the carbon nanoflasks. The magnetic measurements were performed at room temperature using a vibrating sample magnetometer with an applied field of $-1.6\ \mathrm{T} \le H \le 1.6\ \mathrm{T}$. Figure 5 shows the room-temperature hysteresis loop for the acid-treated sample. There is a

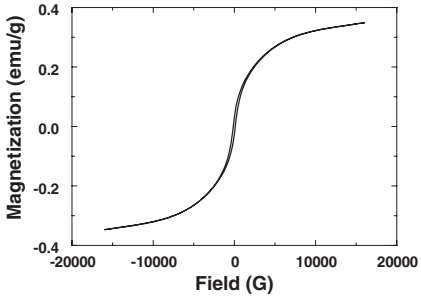

Fig. 5. Plot of magnetization vs. applied field measured for the acid-treated sample.

continuous rise in the magnetization at high magnetic fields, indicating a superparamagnetic type of behavior. Generally, superparamagnetism is seen in the case of nanoparticles of a size below the single domain size of the corresponding material.[15] The presence of hysteresis having a coercivity of 124 G is probably due to a large distribution of particle sizes, as seen from the TEM analyses. The initial susceptibility is sensitive to the presence of larger particles,[15] which exhibit a ferromagnetic behavior. The cobalt-containing nanoflasks, on the other hand, showed a paramagnetic behavior due to the presence of cobalt in the fcc phase.[12] However, since the magnetic properties of the pure MgC_xCo_3 compounds are not yet known, further investigation of the magnetic properties and comparison with that of the bulk compound are necessary in order to understand the correlation between nanostructure and magnetism in these chemically synthesized materials.

In conclusion, a direct catalytic process carried out at 1000 °C resulted in the formation of encapsulated MgC_xCo_3 in carbon nanoflasks, in which the magnetic MgC_xCo_3 particles are well protected by the surrounding graphitic layers. The above phenomenon provides a deeper insight into the mechanism of nanoflask formation, where the role of Mg is found to be crucial to the generation of such a unique shape and structure. The results offer a means to modify the process for the encapsulation of other novel materials, and further exploration of their properties.

Experimental

Synthesis: In a typical preparation, 400 mg of Mg-EtOH powder (prepared by treating fresh Mg powder (Merck) with a mixture of ethanol and water at room temperature (RT) for 48 h and then drying under vacuum) was inserted into a 2 mL closed cell, which was assembled from stainless steel Swagelok parts. Then 700 mg of cobalt tricarbonyl nitrosyl (STREM) was slowly added into the cell by syringe. All the materials were loaded into the cell in an inert atmosphere of nitrogen (glove box). The filled cell was tightly closed and heated in a furnace to 1000 °C at a heating rate of 20 °C min^{-1}. The reaction was continued for 3 h, after which the cell was cooled down to room temperature. The as-synthesized black product obtained from the cell was then treated with a 30 % dilute HCl solution in order to remove the catalytic particles. The resulting purified material was centrifuged, repeatedly washed with de-ionized water and ethanol, and then vacuum dried.

Characterization: The X-ray diffraction patterns of the products were recorded using a Bruker AXS D8 advance powder X-ray diffractometer (using Cu Kα $\lambda = 1.5418$ Å radiation). The TEM images were obtained with a JEOL-JEM 100SX microscope, working at a 100 kV accelerating voltage. Samples for TEM were prepared by dispersing the powdered sample in ethanol by sonication and then drop-drying on a copper grid (400 mesh, electron microscopy sciences) coated with carbon film. Selected area electron diffraction (SAED) and selected area energy dispersive spectral (SAEDAX) analyses were carried out with the respective analyzers attached to a Philips CM-120 TEM instrument. Elemental analysis was done using an Eager 200 CHN analyzer.

Received: November 26, 2002
Final version: February 27, 2003

[1] a) H. Dai, E. W. Wong, Y. Z. Lu, S. Fan, C. M. Lieber, *Nature* **1995**, *375*, 769. b) P. M. Ajayan, S. Iijima, *Nature* **1993**, *361*, 333. c) C. Guerret-Piecourt, Y. Le Bouar, A. Loiseau, H. Pascard, *Nature* **1994**, *372*, 761. d) S. Subramoney, *Adv. Mater.* **1998**, *10*, 1157.

[2] a) Y. Saito, M. Okuda, T. Yoshikawa, A. Kasuya, Y. Nishina, *J. Phys. Chem.* **1994**, *98*, 6696. b) Y. Saito, *Carbon* **1995**, *33*, 979.

[3] a) S. Seraphin, D. Zhou, J Jiao, M. A. Minke, J. C. Withers, R. Loutfy, *Nature* **1993**, *362*, 503. b) S. Seraphin, D. Zhou, J. Jiao, *J. Appl. Phys.* **1996**, *80*, 2097.

[4] a) R. S. Ruoff, D. C. Lorents, B. Chan, R. Malhotra, S. Subramoney, *Science* **1993**, *259*, 346. b) S. Subramoney, R. S. Ruoff, D. C. Lorrents, R. Malohotra, *Nature* **1993**, *366*, 637.

[5] a) Z. Turgut, J. H. Scott, M.-Q. Huang, S. A. Majetich, M. E. McHenry, *J. Appl. Phys.* **1998**, *83*, 6468. b) S. A. Majetich, J. Q. Artman, M. E. McHenry, N. T. Nuhfer, S. W. Staley, *Phys. Rev. B* **1993**, *48*, 16 845.

[6] a) R. Sen, A. Govindaraj, C. N. R. Rao, *Chem. Mater.* **1997**, *9*, 2078. b) P. J. F. Harris, S. C. Tsang, *Chem. Phys. Lett.* **1998**, *293*, 53. c) N. Grobert, W. K. Hsu, Y. Q. Zhu, J. P. Hare, H. W. Kroto, M. Terrones, H. Terrones, P. Redlich, M. Ruhle, R. Escudero, F. Morales, *Appl. Phys. Lett.* **1999**, *75*, 3363.

[7] a) T. Kyotani, L.-F. Tsai, A. Tomita, *Chem. Commun.* **1997**, 701. b) G. Che, B. B. Lakshmi, E. R. Fischer, C. R. Martin, *Nature* **1998**, *393*, 346.

[8] a) S. C. Tsang, Y. K. Chen, P. J. F. Harris, M. L. H. Green, *Nature* **1994**, *372* 159. b) J. Sloan, M. Terrones, S. Nufer, S. Friedrichs, S. R. Bailey, H. G. Woo, M. Rühle, J. L. Hutchison, M. L. H. Green, *J. Am. Chem. Soc.* **2002**, *124*, 2116.

[9] T. He, Q. Huang, A. P. Ramirez, Y. Wang, K. A. Ragan, N. Rogado M. A. Hayward, M. K. Haas, J. S. Slusky, K. Inumara, H. W. Zandbergen, N. P. Ong, R. J. Cava, *Nature* **2001**, *411*, 54.

[10] S. Liu, X. Tang, L. Yin, Y. Koltypin, A. Gedanken, *J. Mater. Chem.* **2000**, *10*, 1271.

ADVANCED MATERIALS

[11] R. K. Rana, A. Gedanken, *J. Phys. Chem. B* **2002**, *106*, 9769.
[12] The typical morphology of carbon nanoflasks in an enriched sample displayed by various microscopes can be found in: S. Liu, S. Boeshore, A. Fernandez, M. J. Sayagues, J. E. Fischer, A. Gedanken, *J. Phys. Chem. B* **2001**, *105*, 7606.
[13] L. J. Huetter, H. H. Stadelmaier, *Acta Metall.* **1958**, *6*, 367.
[14] a) R. K. Rana, Y. Koltypin, A. Gedanken, *Chem. Phys. Lett.* **2001**, *344*, 256. b) R. K. Rana, X. N. Xu, Y. Yeshurun, A. Gedanken, *J. Phys. Chem. B* **2002**, *106*, 4079.
[15] D. L. Leaslie-Pelecky, R. D. Rieke, *Chem. Mater.* **1996**, *8*, 1770.

Soluble Microcapsules Assembled Stepwise from Weak Polyelectrolytes Using Acid-Decomposable Cores**

By *Changyou Gao*,* *Helmuth Möhwald*, and *Jiacong Shen*

Hollow capsules are of both scientific and technological interest because of their potential applications as new colloidal structures in areas such as medicine, drug delivery, artificial cells or viruses, and catalysis.[1] Layer-by-layer (LBL) assembly of oppositely charged polyelectrolytes[2] onto removable colloidal particles has been used to create novel hollow nano- and microcapsules.[3] This fabrication technique allows control of the capsule size and shape, the capsule wall thickness, and the capsule wall composition. Microcapsules with customized physicochemical properties can be obtained by incorporating one or more functional components such as nanoparticles, biomacromolecules, lipids, photosensitive dyes, inorganic crystals, and multivalent ions onto the capsule wall or into the capsule interior.[4]

The typical hollow capsules produced so far are composed of poly(styrenesulfonate sodium salt) (PSS)/poly(allylamine hydrochloride) (PAH), PSS/poly(diallyldimethyl ammonium chloride) (PDADMAC), or PSS/chitosan. Weakly crosslinked melamine formaldehyde (MF) colloidal particles or red blood cells have often been employed as sacrificial templates. After the desired number of layers has been deposited, the MF cores or the red blood cells are routinely decomposed in a solution of low pH (< 1.6) or deproteinizer, respectively.[3a,5] These harsh conditions may destroy the multilayers if the association between the negatively and positively charged species is not strong enough. Hence, at least one strong polyelectrolyte in the oppositely charged pairs is generally employed to obtain capsules with high integrity.

Much effort has been devoted to the nanoscale encapsulation of drugs, minerals, dyes, proteins, enzymes, and genes.[6] However, entities with large geometric size and/or rigid structure such as nanoparticles and macromolecules of ultrahigh molecular weight are difficult to incorporate unless one takes specific measures to open the capsules. To create microcapsules with controllable permeability, attention has been paid to microcapsules of weak polyelectrolytes, where the charge density on the capsule wall can be readily controlled by adjusting the pH values of the bulk solutions. With this class of systems, exemplified by poly(acrylic acid) (PAA) and PAH, pH-modulated permeability can be expected as a result of conformation alteration of the macromolecular chains.[7] Moreover, it has been reported that pores in the range of hundreds of nanometers on PAA/PAH multilayers assembled at some pH values have been created as a result of phase separation induced by pH change or salt exposure.[7a,8] Due to the weak bonding, dissolution of the formed capsules at mild pH conditions is also possible. Therefore, one obtains greater control over the physical state of the assembled capsules, such as pH-tuned opening or closure, surface texture, and solubility.

In this communication we describe the successful fabrication of weak polyelectrolyte microcapsules by consecutive adsorption of PAA and PAH onto MF colloidal particles, followed by decomposition of MF cores in 0.1 M HCl solution. Given the fast core decomposition rate, the technical problem of shell dissolution was solved by precise control of the time of treatment in acid solution. The resulting microcapsules are readily soluble at low pH. Microcapsules with porous wall texture were achieved by depositing PAA and PAH stepwise onto fluorescein diacetate (FDA) crystals at pH 3.5 and 7.5, respectively, followed by treatment at pH 2.5 and then dissolution of FDA by acetone.

To monitor the process of film formation, i.e., charge reversal at each step, by electrophoresis, MF particles with a diameter of 500 nm were alternately coated with PAA (molecular weight M_w 5100) and PAH in 0.5 M NaCl solution (without adjusting pH values).[9] After adsorption for 10 min, three washings were carried out to remove excess polyelectrolytes. Figure 1 summarizes the ζ-potential recorded upon layer deposition for PAA/PAH pairs. The ζ-potential alternates between positive and negative values, indicating the successful recharging of the particles coated with the adsorbed polyelectrolyte multilayers upon each layer deposition.

Acid-decomposable MF particles with an average size of 3.7 μm were employed as templates to prepare PAA/PAH hollow microcapsules. All coatings and washings were continuously conducted in 0.2 M NaCl solution with polyelectrolyte concentration of 2 mg/mL, where the natural pH values for PAA (M_w 20 000) solution and PAH solution are 7.7 and 4.7, respectively.[10] A lower salt concentration would be favorable to obtain denser multilayers on the colloidal particle surface. Moreover, by using PAA with larger molecular weight, a shell structure more stable against acid dissolution during the core removal procedure is expected, owing to the higher chance of entanglement between molecular chains.

After five bilayers of PAA/PAH had been deposited, the coated particles were treated with 0.1 M HCl solution. How-

[*] Prof. C. Y. Gao, Prof. J. C. Shen
Department of Polymer Science and Engineering, Zhejiang University
Hangzhou, 310027 (P.R. China)
E-mail: cygao@mail.hz.zj.cn
Prof. H. Möhwald
Max Planck Institute of Colloids and Interfaces
D-14424, Potsdam (Germany)

[**] Financial support by the Natural Science Foundation of China (90206006) is gratefully acknowledged. We thank A. Heilig and H. Zastrow for their assistance with the SFM and ζ-potential measurements. C. Y. Gao thanks the Max Planck Society for a visiting scientist grant.

  DOI: 10.1002/adma.200304667